INORGANIC CHEMISTRY FRONTIERS

RESEARCH ARTICLE

View Article Online
View Journal | View Issue

Cite this: *Inorg. Chem. Front.*, 2025, **12**, 1437

Tin chalcohalide $Sn_{11}(PS_4)_4I_{10}$ obtained from structural-template-oriented synthesis: exhibiting balanced infrared nonlinear optical performance†

Cuier Deng,‡[a,b] Xi Xu,‡[a] Yuhan Hu,[a,b] Jingyu Guo,*[a,b] Li-Ming Wu *[a,b] and Ling Chen *[a,b]

Received 31st October 2024,
Accepted 18th December 2024

DOI: 10.1039/d4qi02753a

rsc.li/frontiers-inorganic

Among infrared (IR) nonlinear optical (NLO) materials, metal chalcohalides have become prominent because of their well-balanced performance and are widely applied in optoelectronics, communications, and sensor technology. Structural-template-oriented synthesis is an important method in the exploration of metal chalcohalides, mainly focusing on anion/cation substitution, co-substitution and structure prediction. Herein, a novel tin chalcohalide, $Sn_{11}(PS_4)_4I_{10}$ (SPSI), has been successfully obtained via structural-template-oriented synthesis, utilizing the excellent and suitable structural template Pb_2BO_3X (X = halogens) family. SPSI satisfies the requirements of an excellent IR NLO material as a balanced-performance pentagonal candidate, including a moderate second-harmonic generation (SHG) response (0.8 × AGS), a wide IR transparency window (0.46–17.6 μm), a suitable $\Delta n_{obv.}$ value (0.068 at 546 nm) and a considerable laser-induced damage threshold (LIDT) (3.3 × AGS).

Introduction

Nonlinear optical (NLO) crystals serve as the core optical components of solid-state lasers for outputting frequency-doubled lasers through second-harmonic generation (SHG),[1–3] which broadens the laser wavelength and extends the application range. Over the past decades, several excellent NLO crystals ranging from ultraviolet (UV) to infrared (IR) spectral regions have been designed and synthesized,[4–9] including β-BaB_2O_4 (BBO), LiB_3O_5 (LBO), $CsLiB_6O_{10}$ (CLBO), KH_2PO_4 (KDP), $KTiOPO_4$ (KTP), $KBe_2BO_3F_2$ (KBBF), $NH_4B_4O_6F$ (ABF), $AgGaS_2$ (AGS), $AgGaSe_2$ (AGSe) and $ZnGeP_2$ (ZGP). Undesirably, some intrinsic drawbacks remain a large obstacle to high-power laser applications, such as the unsatisfactory laser-induced damage threshold (LIDT) for AGS and AGSe, as well as adverse two-photon absorption (about 1 μm) for ZGP (E_g = 1.47 eV). Therefore, there is an urgent demand for the design and synthesis of IR NLO crystals with balanced performance.

Generally, a promising IR NLO crystal for various applications requires the following conditions: (1) a large SHG coefficient ($d_{ij} \geq 6.7$ pm V^{-1}) that is about half of AGS; (2) a multi-waveband IR transparency window, especially two important atmospheric windows (3–5 and 8–12 μm); (3) a high LIDT (≥2.0 × AGS) for high-power laser applications; (4) a suitable birefringence Δn (>0.03) to satisfy phase matching; and (5) nontoxic, stable physical and chemical properties for good crystal growth.[10,11] Thus, a compound must satisfy all these requirements simultaneously, which is demanding and challenging.

Metal chalcogenides, such as Ga_2S_3,[12] Li_3PS_4,[13] $RbPbPS_4$ [14] and $SrZnGeS_4$,[15] have become the focus of exploration because of their diversity in chemical bonding and bonding connection. Considering AGS as a template, these compounds have similar diamond-like crystal structures that can be regarded as being designed from the primary $[MS_4]$ (M = metal, Si and P) tetrahedral building unit. With further exploration in recent decades, metal chalcohalides stand out from the crowd, inheriting the intrinsic advantages of both chalcogenides and halides. Because of the halogen involvement, it can drive the generation of a more flexible and highly polarizable structure to achieve a balance between the wide optical band gap, large SHG coefficient and birefringence, such as $[ABa_3Cl_2][Ga_5S_{10}]$ (A = K, Rb, and Cs),[16] $NaBa_4Ge_3S_{10}Cl$,[17] $Cs_4Zn_5P_6S_{18}I_2$ [18] and $[Sr_4Cl_2][Si_3S_9]$.[19] However, the main approaches used to explore

[a]*Faculty of Arts and Sciences, Beijing Normal University, Zhuhai 519087, People's Republic of China*
[b]*Beijing Key Laboratory of Energy Conversion and Storage Materials, College of Chemistry, Beijing Normal University, Beijing 100875, People's Republic of China*

†Electronic supplementary information (ESI) available: Experimental sections, computational methods, crystallographic data tables, powder XRD patterns, and optical property measurements for $Sn_{11}(PS_4)_4I_{10}$. CCDC 2384809 for $Sn_{11}(PS_4)_4I_{10}$. For ESI and crystallographic data in CIF or other electronic format see DOI: https://doi.org/10.1039/d4qi02753a

‡These authors contributed equally to this work.

metal chalcohalides are anion/cation substitution and co-substitution at present. There is a lack of excellent and suitable structural templates for designing chalcohalide IR NLO crystals.

Considering oxygen–sulfur substitution, several excellent structural templates in UV NLO oxysalt halides were taken as a worthy reference for designing IR NLO chalcohalides.[20,21] Guided by this strategy, the crystal structure of Pb_2BO_3X (X = Cl, Br and I) was regarded as a design template. This Pb_2BO_3X phase exhibits a pseudo-layered structure, and the interlayer anion (halogen), anion unit ($[BO_3]^{3-}$) and cation (Pb^{2+}) exhibit high structural tolerance and alternative flexibility. Through this design template, many new compounds are obtained, such as Pb_2BO_3I[22] exhibiting a large SHG response of approximately 10 × KH_2PO_4 (KDP) and flexible Sn_2PO_4I[23] exhibiting a large Δn value of 0.664 at 546 nm, which exceeds those of the reported borates and phosphates.

In this study, a novel tin chalcohalide, $Sn_{11}(PS_4)_4I_{10}$ (SPSI), was obtained successfully using this template. Remarkably, SPSI satisfies the requirements of an excellent IR NLO material as a balanced-performance pentagonal candidate and demonstrates a moderate SHG response (0.8 × AGS), a wide IR transparency window (0.46–17.6 μm), a suitable $\Delta n_{obv.}$ value (0.068 at 546 nm) and a considerable LIDT (3.3 × AGS).

Experimental section

Light yellow crystals of SPSI were synthesized using a high-temperature solid-state reaction in a closed system. A mixture of SnS, SnI_2, and P_2S_5 (molar ratio of about 4 : 4 : 1, 0.3 g in total) was fully ground and loaded into a silica tube, and then the tube was gradually heated to 300 °C, 500 °C and 720 °C in 5 h and held for 5 h at each temperature. Afterward, the tube was cooled slowly to 20 °C at a rate of 0.5 °C min^{-1}. The extra SnS and SnI_2 also function as fluxes. We also found that P_2S_5 can also be used as a flux. Block-shaped and light yellow crystals with sizes of about 0.130 × 0.092 × 0.045 mm^3 (Fig. 1f) were obtained.

A yellow polycrystalline sample of SPSI was synthesized similar to the above methods. A tube containing a mixture of SnS, SnI_2 and P_2S_5 (molar ratio of about 6 : 5 : 2, 0.3 g in total) was heated to 350 °C for 1 h and held at this temperature for 3 h. The yield was 100%. The experimental powder X-ray diffraction peaks of SPSI are fully indexed, ensuring the purity of the sample (Fig. 1g).

Other experimental details, including UV/vis-NIR diffuse-reflectance spectroscopy, property measurements (SHG, birefringence, LIDT), thermal analysis and theoretical calculations, are listed in the ESI.†

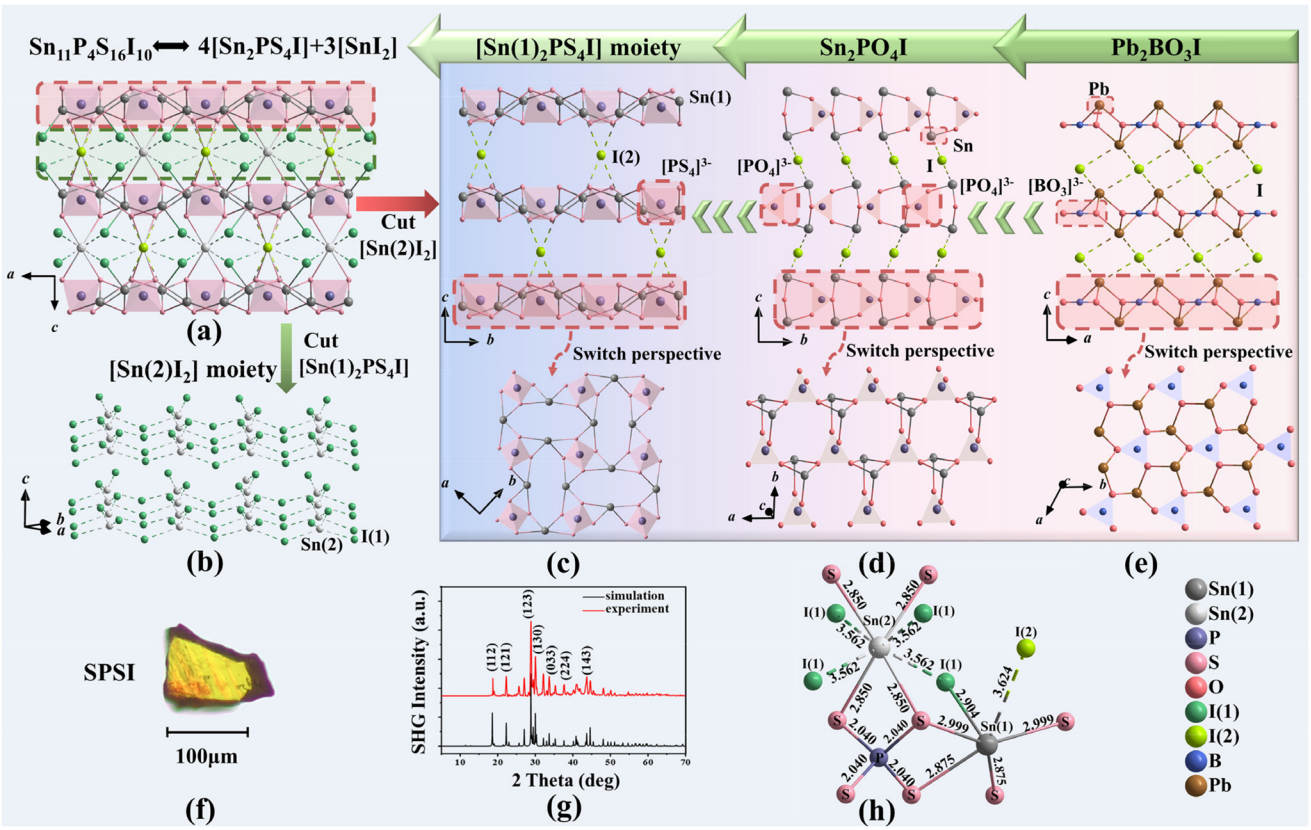

Fig. 1 (a) The crystal structure of $Sn_{11}(PS_4)_4I_{10}$ (SPSI). (b) The $[Sn(2)I_2]$ moiety; structural evolution of (c) the $[Sn(1)_2PS_4I]$ moiety from (d) Sn_2PO_4I and (e) Pb_2BO_3I. (f) The SPSI crystal under a microscope with a size of approximately 0.130 × 0.092 × 0.045 mm^3. (g) The PXRD pattern of SPSI. (h) The asymmetric unit of SPSI with the bond length marked (Å).

Results and discussion

Crystal structure description and comparison

SPSI crystallizes in a noncentrosymmetric (NCS) tetragonal space group $I\bar{4}2m$ (no. 121), with the following cell parameters: a = 9.3157(4) Å, b = 9.3157(4) Å, c = 13.8689(13) Å, V = 1203.57 (15) Å^3, Z = 1, and CCDC 2384809.† The crystallographic and structure refinement data are listed in Tables S1–S3 (ESI).† As shown in Fig. 1a, SPSI exhibits a 3D structure that consists of two parts: one is the $[SnPS_4I]$ moiety, which is similar to the Pb_2BO_3X template, and the other is the $[SnI_2]$ substructure. These two components are interleaved, forming a 3D structure by sharing I and S atoms.

In the unit cell, there are two crystallographically independent Sn atoms, one P atom, one S atom and two unique I atoms (Fig. 1 and Table S3†). The P(1) atom is located on the 4d Wyckoff site with a site symmetry of $\bar{4}$, adopting a $[PS_4]$ tetrahedral coordination with a P–S bond length of 2.040(4) Å and S–P–S bond angles ranging from 108.9 to 110.5°. The Sn(1) atom is six-coordinated with four S(1) atoms, one I(1) atom and one I(2) atom to form the $[Sn(1)S_4I(1)I(2)]^{8-}$ polyhedron, where the bond lengths of Sn(1)–S(1) and Sn(1)–I(1) are 2.88–3.00 Å and 2.90 Å, respectively. All these bond lengths and bond angles are within reasonable bond lengths. Differently, the Sn (2) atom is eight-coordinated with four S(1) atoms and four I(1) atoms to form the $[Sn(2)S(1)_4I(1)_4]^{10-}$ polyhedron with Sn(2)–S (1) = 2.850(4) Å and Sn(2)–I(1) = 3.562(13) Å.

The bond valence sum (BVS) data are studied, the BVS is 0.87 of I(1), but merely 0.38 of I(2) in Table S3.† These are caused by their different coordination environments. I(2) is four coordinated by four Sn(1) atoms with a relatively longer Sn(1)–I(2) bond length of 3.624 Å and located within the channel (Fig. 1c), which indicates weaker bonding interactions and a lower BVS value. Such a structural motif has also been seen in other related compounds, for example, Sb_5O_7I, where the Sb–I bond length is 3.93–3.86 Å, and the BVS of I is 0.52;[24] and Sn_2PO_4I, where Sn–I = 3.43 Å, and the BVS of I is 0.4.[23]

Interestingly, the molecular formula of $Sn_{11}(PS_4)_4I_{10}$ can be regarded as merging three $[SnI_2]$ and four $[Sn_2PS_4I]$. Therefore, the crystal structure of SPSI is also composed of two moieties, $[Sn(2)I_2]$ and $[Sn(1)_2PS_4I]$. The $[Sn(1)_2PS_4I]$ moiety can be regarded as the framework of the structure, while the $[Sn(2)I_2]$ moiety acts as a filler between $[Sn(1)_2PS_4I]$ layers to reinforce and prop up the architecture, and the two moieties complement each other to form SPSI. The $[Sn(2)I_2]$ substructure is shown in Fig. 1b, which is a net-like $[Sn(2)I(1)_2]_\infty$ layer extending along the *ab* plane, within which the Sn(2) forms a $[SnI_4]^{2-}$ tetrahedron that is linked with each other by sharing corner I(1) atoms, whereas the $[Sn(1)_2PS_4I]$ moiety is regarded as evolving from the Pb_2BO_3I template.[22] As shown in Fig. 1c–e, the correlation and development from the Pb_2BO_3I template to Sn_2PO_4I[23] and to the $[Sn(1)_2PS_4I]$ moiety are depicted. The $[Sn(1)_2PS_4]_\infty^+$ layers are linked by the interlayer I^- anions, which is similar to the layered characteristic of the Pb_2BO_3I template (Fig. 1e). In this scenario, the Sn(1) atom functions as a Pb atom in the template, and the PS_4 tetrahedron acts as the building unit of the BO_3 triangle. Such a chemical co-substitution drives the evolution from Pb_2BO_3I[22] to Sn_2PO_4I,[23] and finally to the $[Sn_2PS_4I]$ moiety in SPSI. The same corner-sharing connection between different building units remains. More interestingly, besides the similarity of the structure preserved from the Pb_2BO_3I template, the nonlinear optical properties seem to have been inherited.

Optical and SHG performance

The SHG responses of SPSI and AGS were measured using a 2100 nm pulse (1 Hz, 10 ns) laser with polycrystalline samples with particle sizes ranging from 50 μm to 250 μm. As shown in Fig. 2a, the SHG response of SPSI is approximately 0.8 × AGS with the sample particle size. This intensity is comparable with that of $Pb_{3.5}GeS_4Br_3$ (0.8 × AGS),[25] and is stronger than those of Sn-containing thiophosphates, *i.e.*, $KSnPS_4$ (0.55 × AGS), $RbSnPS_4$ (0.45 × AGS), and $CsSnPS_4$ (0.4 × AGS).[26] Notably, the SHG intensities of SPSI exhibit a growing trend as particle sizes increase, suggesting phase-matching (PM) behavior.

Under a ZEISS Axio polarizing microscope,[27] the delay value for full extinction R at 546 nm is 0.898 μm utilizing the as-grown crystals of SPSI (13.2 μm in thickness). The refractive index difference was found to be 0.068 at 546 nm. It is consistent with the phase-matching capability probably.

As shown in Fig. 2b, IR spectroscopic analysis of SPSI revealed an absorption peak at 17.6 μm, which was attributed to the inherent absorption of chemical P–S bonds. No obvious absorption peak is observed within the spectral range of 2.5 to 17.6 μm, implying that compound SPSI does not exhibit significant absorption within this region and suggesting a wide infrared cutoff-edge reaching up to 17.6 μm, thus indicating its

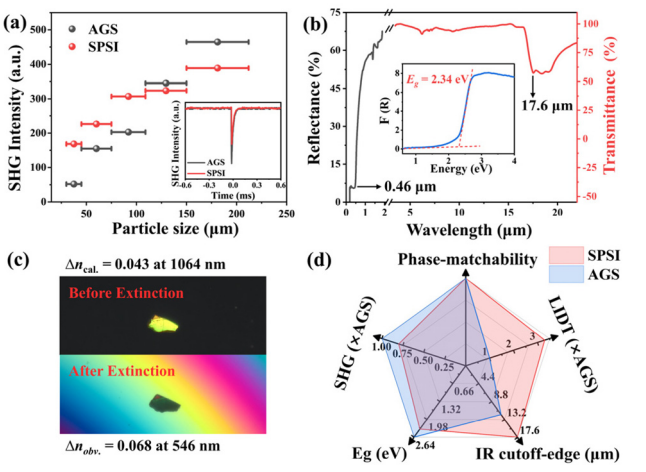

Fig. 2 (a) The SHG intensities of SPSI and AGS at 2100 nm. (b) Optical transparency range (0.25–2.0 μm: UV/vis-NIR diffuse reflectance spectroscopy; 2.0–22 μm: IR spectroscopy). (c) The photograph of the SPSI crystal before and after extinction observed during birefringence measurement using a Berek compensator. (d) The corresponding radar chart of phase-matchability, SHG effect, E_g value, IR transparent window and LIDT for SPSI and AGS.

potential suitability for applications in the middle or even far-IR ranges. This extensive transparent region of SPSI is almost larger than that of other IR-NLO compounds, such as AGS (~11 μm),[14] $Hg_3P_2S_8$ (~16.3 μm)[28] and $CuZnPS_4$ (~16.5 μm).[29]

The Kubelka–Munk[30] function value of the compound SPSI is 2.34 eV (Fig. 2b inside), which is consistent with the yellow appearance and is similar to those of AGS (2.64 eV),[31] Ag_3PS_4 (2.43 eV),[32] $SbPS_4$(2.54 eV),[33] $Na_6Sn_3P_4S_{16}$(2.52 eV)[34] and $KSnPS_4$ (2.2 eV).[26] According to the "Electronic Structure Engineer Bucket Effect Theory",[35] the band gap (E_g) of a compound is primarily determined by "the shortest E_g board" among its components, which can be roughly estimated based on the band gaps of the corresponding binary compounds. For example, due to the trend in binary compound band gaps: SnS (1.07 eV) < SnI_2 (2.45 eV) < P_2S_5 (2.54 eV),[36–38] the band gap of the compound SPSI (2.34 eV), formed from these components, is practically comparable to that of SnS. Similarly, for seemingly diverse compounds such as AGS, Ag_3PS_4, $SbPS_4$, $Na_6Sn_3P_4S_{16}$, and $KSnPS_4$, the shortest E_g board is Ag_2S (0.92 eV), Sb_2S_3 (1.64 eV), and SnS (1.07 eV), respectively. Thus, these compounds, despite having significantly different constituent structures, exhibit similar band gap values. Usually, for IR NLO compounds, the bandgap is proportional to the LIDT, and a wider bandgap is more advantageous for enhancing the LIDT. The powder SPSI sample exhibited an LIDT of 11.3 MW cm^{-2} using a laser of 1.06 μm, and the strong laser damage resistance was approximately 3.3 times greater than that of AGS (3.4 MW cm^{-2}) under the same measurement conditions. In addition, SPSI remains stable at 240 °C as shown by the TG-DSC curve (Fig. S2†).

Briefly, SPSI is a promising nonlinear optical crystal with balanced performance in the mid-far infrared compared with AGS.

Theoretical calculations

To deeply clarify the bonding features and the possible physical origin of the optical properties of SPSI, first-principles calculations were performed to assess electronic structures and optical properties. It is noteworthy that the average occupancy of Sn atoms in the Sn(2) site is 0.75 (Table S3†). Therefore, the structure of SPSI could be disordered and requires special treatment in modeling. We extended the unit cell of SPSI to form different configurations and select the most stable configuration in energy as the representative configuration for the following first-principles calculations. The projected densities of states (PDOS) of the representative configurations for the SPSI are shown in Fig. 3a. The conduction band minimum (CBM) is mainly composed of the 5p states of Sn atoms, the 3p states of S atoms, and the 5p states of I atoms. Besides, the valence band maximum (VBM) is constituted by the 5s states of Sn atoms, the 3p states of S atoms, and the 5p states of I atoms. From the negative partial crystal orbital Hamiltonian population (pCOHP) in Fig. 3a, near the Fermi level, the Sn–S interactions have a larger antibonding region than the Sn–I interactions. Thus, these findings suggest that the Sn–S bonds have stronger covalent interactions than the Sn–I bonds.

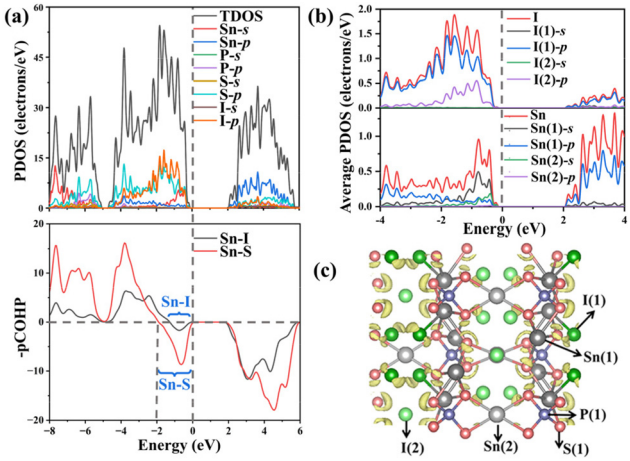

Fig. 3 (a) The PDOS and −pCOHP of SPSI. (b) The PDOS of Sn(1), Sn(2), I(1) and I(2) divided by the number of atoms in a cell. (c) The electron distribution.

Furthermore, the 5p states of Sn(1), Sn(2), I(1) and I(2) sites are shown in Fig. 3b, respectively. In both the CBM and VBM, the densities of the states of Sn(1) and I(1) are greater than that of Sn(2) and I(2). This finding demonstrates that Sn(1) and I(1) may contribute more to the optical properties, which can be further confirmed by the electron localization functions in Fig. 3c. On the one hand, as shown in Fig. 3c, S(1) and I(1) have greater electron distributions than other atoms, especially I(2). This shows that the stereochemical activity of lone pairs of Sn(2) is not exerted, and the outer electrons of S(1) and I(1) exert a great influence on the optical properties. On the other hand, as shown in Fig. S3,† the Sn(1) atoms present a weak asymmetric electron distribution, whereas the Sn(2) atoms present no electron distribution. Since the stereochemically active lone pairs of Sn(1) is stronger than those of Sn(2), the $[Sn(1)_2PS_4I]$ moiety may be the main contributor to the optical properties of SPSI. Meanwhile, the $[Sn(2)I_2]$ moiety synergistically improves the optical properties of SPSI.

The calculated band structure indicates that SPSI is an indirect band gap compound with theoretical band gaps of 1.68 eV (Fig. S4†) using PBE[39,40] and 2.26 eV using HSE06.[41,42] Additionally, the calculated birefringence is 0.043 at 1064 nm, as shown in Fig. S4,† where a suitable birefringence is also consistent with phase matching. In addition, considering that the point group of SPSI belongs to $I\bar{4}2m$, one nonvanishing independent SHG tensor (d_{36}) is identified under the restriction of the Kleinman symmetry. Compared with AGS (d_{36} = 13.4 pm V^{-1}), the calculated maximum tensor d_{36} of SPSI is 13.9 pm V^{-1} (1 × AGS), which also supports the experimental observation (0.8 × AGS).

Conclusions

In conclusion, a new IR-NLO crystal $Sn_{11}(PS_4)_4I_{10}$ (SPSI), a tin chalcohalide, was successfully synthesized with the guidance

of structural-template-oriented synthesis. Its structure features a 3D framework constructed using two substructures, the [Sn(2)I_2] moiety and [Sn_2PS_4I] moiety, where the [$Sn(1)_2PS_4I$] moiety is structurally like the Pb_2BO_3I template. SPSI exhibits a phase-matching SHG response (0.8 × AGS), a wide infrared transparent window (0.46–17.6 μm), an appropriate bandgap (2.34 eV), a suitable birefringence (0.068 at 546 nm) and a high LIDT (3.3 × AGS). In-depth theoretical calculations indicate that the [$Sn(1)_2PS_4I$] moiety is the dominant contributor and the [Sn(2)I_2] moiety makes a synergistic contribution to improving the optical performance of SPSI. This research reveals a structural-template-oriented development of otherwise unrelated compounds, enhancing our understanding of the microscopic structure and bulk properties and providing a novel approach for future design, synthesis and exploration of high-performance functional materials.

Author contributions

J. Y. G., C. E. D., Y. H. H., L. M. W., and L. C. conceived, designed and performed all experimental work. X. X. developed the theory. L. C., J. Y. G. and C. E. D. wrote the draft paper. All the authors discussed the results and commented on the manuscript. All authors contributed to the general discussion.

Data availability

The authors confirm that the data supporting the findings of this study are available within the article [and/or] its ESI.†

Conflicts of interest

There are no conflicts to declare.

Acknowledgements

This work was supported by the National Natural Science Foundation of China (22205024 and 22193043), the Interdisciplinary Intelligence Supercomputer Center of Beijing Normal University, Zhuhai, and the Instrumentation and Service Center for Science and Technology, Beijing Normal University, Zhuhai.

References

1 X. Liu, Y. C. Yang, M. Y. Li, L. Chen and L. M. Wu, Anisotropic structure building unit involving diverse chemical bonds: A new opportunity for high-performance second-order NLO materials, *Chem. Soc. Rev.*, 2023, **52**, 8699–8720.

2 M. Mutailipu and S. L. Pan, Emergent deep-ultraviolet nonlinear optical candidates, *Angew. Chem., Int. Ed.*, 2020, **59**, 20302.

3 K. M. Ok, Toward the rational design of novel noncentrosymmetric materials: Factors influencing the framework structures, *Acc. Chem. Res.*, 2016, **49**, 2774–2785.

4 G. M. Li, Z. H. Yang, X. L. Hou and S. L. Pan, Chain-like [S_x] (x = 2-6) units realizing giant birefringence with transparency in the near-infrared for optoelectronic materials, *Angew. Chem., Int. Ed.*, 2023, **62**, e202303711.

5 P. F. Li, C. L. Hu, B. X. Li, J. G. Mao and F. Kong, From $CdPb_8(SeO_3)_4Br_{10}$ to $Pb_3(TeO_3)Br_4$: The first tellurite bromide exhibiting an SHG response and mid-IR transparency, *Inorg. Chem. Front.*, 2023, **10**, 7343–7350.

6 J. Y. Guo, X. T. Zhan, J. T. Lan, X. Liu, S. Zhao, X. Xu, L. M. Wu and L. Chen, $Sb_4O_5I_2$: Enhancing birefringence through optimization of Sb/I ratio for alignment of stereochemically active lone pairs, *Inorg. Chem.*, 2024, **63**, 2217–2223.

7 C. T. Chen, B. C. Wu, A. D. Jiang and G. M. You, A new-type ultraviolet SHG crystal: β-BaB_2O_4, *Sci. Sin., Ser. B*, 1985, **28**, 235–243.

8 T. Sasaki and A. Yokotani, Growth of large KDP crystals for laser fusion experiments, *J. Cryst. Growth*, 1990, **99**, 820–826.

9 B. Tell and H. M. Kasper, Optical and electrical properties of $AgGaS_2$ and $AgGaSe_2$, *Phys. Rev. B*, 1971, **4**, 4455–4459.

10 S. D. Yang, C. S. Lin, H. X. Fan, K. C. Chen, G. Zhang, N. Ye and M. Luo, Polar phosphorus chalcogenide cage molecules: Enhancement of nonlinear optical properties in adducts, *Angew. Chem., Int. Ed.*, 2023, **62**, e202218272.

11 Y. Q. Li, J. H. Luo and S. G. Zhao, Local polarity-induced assembly of second-order nonlinear optical materials, *Acc. Chem. Res.*, 2022, **55**, 3460–3469.

12 M. J. Zhang, X. M. Jiang, L. J. Zhou and G. C. Guo, Two phases of Ga_2S_3: Promising infrared second-order nonlinear optical materials with very high laser induced damage thresholds, *J. Mater. Chem. C*, 2013, **1**, 4754–4760.

13 R. Mercier, J. P. Malugani, B. Fahys, G. Robert and J. Douglade, Structure du tetrathiophosphate de lithium, *Acta Crystallogr.*, 1982, **38**, 1887–1890.

14 A. Y. Wang, S. H. Zhou, M. Y. Ran, B. X. Li, X. T. Wu, H. Lin and Q. L. Zhu, $RbPbPS_4$: A promising IR nonlinear optical material achieved by lone-pair-cation-substitution-induced structure transformation, *Inorg. Chem. Front.*, 2024, **11**, 3744–3754.

15 Q. Q. Liu, X. Liu, L. M. Wu and L. Chen, $SrZnGeS_4$: A dual-waveband nonlinear optical material with a transparency spanning UV–vis and far-IR spectral regions, *Angew. Chem., Int. Ed.*, 2022, **61**, e202205587.

16 B. W. Liu, H. Y. Zeng, X. M. Jiang and G. C. Guo, Phase matching achieved by bandgap widening in infrared nonlinear optical Materials [ABa_3Cl_2][Ga_5S_{10}] (A = K, Rb, and Cs), *CCS Chem.*, 2021, **3**, 964–973.

17 K. Feng, L. Kang, Z. S. Lin, J. Y. Yao and Y. C. Wu, Noncentro-symmetric chalcohalide $NaBa_4Ge_3S_{10}Cl$ with large band gap and IR NLO response, *J. Mater. Chem. C*, 2014, **2**, 4590–4596.

18 X. D. Chai, M. Z. Li, S. J. Lin, W. F. Chen, X. M. Jiang, B. W. Liu and G. C. Guo, $Cs_4Zn_5P_6S_{18}I_2$: The largest birefringence in chalcohalide achieved by highly polarizable nonlinear optical functional motifs, *Small*, 2023, **19**, 2303847.

19 C. Y. Zhao, K. Wu, Y. Xiao, B. B. Zhang, H. H. Yu and H. J. Zhang, $[Sr_4Cl_2][Si_3S_9]$: Ultrawide-bandgap salt-inclusion thiosilicate nonlinear optical material with unprecedented tripolymerized $[Si_3S_9]$ clusters, *J. Mater. Chem. C*, 2023, **11**, 4439–4443.

20 J. K. Wang, Y. S. Cheng, H. P. Wu, Z. G. Hu, J. Y. Wang, Y. C. Wu and H. W. Yu, $Sr_3[SnOSe_3][CO_3]$: A heteroanionic nonlinear optical material containing planar π-conjugated $[CO_3]$ and heteroleptic $[SnOSe_3]$ anionic groups, *Angew. Chem., Int. Ed.*, 2022, **61**, e202201616.

21 Z. Qian, H. P. Wu, Z. G. Hu, J. Y. Wang, Y. C. Wu and H. W. Yu, $Cs_3In(In_4Se_7)(P_2Se_6)$: A multi-chromophore chalcogenide with excellent nonlinear optical property designed by group grafting, *Angew. Chem., Int. Ed.*, 2024, **63**, e202400892.

22 H. W. Yu, N. Z. Koocher, J. M. Rondinelli and P. S. Halasyamani, Pb_2BO_3I: A borate iodide with the largest second-harmonic generation (SHG) response in the $KBe_2BO_3F_2$ (KBBF) family of nonlinear optical (NLO) materials, *Angew. Chem., Int. Ed.*, 2018, **57**, 6100.

23 J. Y. Guo, A. Tudi, S. J. Han, Z. H. Yang and S. L. Pan, Sn_2PO_4I: An excellent birefringent material with giant optical anisotropy in non π-conjugated phosphate, *Angew. Chem., Int. Ed.*, 2021, **60**, 24901.

24 M. Yang, W. L. Liu and S. P. Guo, Sb_5O_7I: Exploration of ternary antimony-based oxyhalide as a nonlinear-optical material, *Inorg. Chem.*, 2022, **61**, 14517–14522.

25 J. Z. Zhou, H. S. Wang, J. J. Liu, X. Su, Y. Chu, J. Qu and X. Z. Jiang, $Pb_{3.5}GeS_4Br_3$: The first phase-matching thiogermanate halide infrared nonlinear optical material, *Inorg. Chem. Front.*, 2024, **11**, 2681–2689.

26 Y. Huang, D. D. Chu, Y. Zhang, C. W. Xie, G. M. Li and S. L. Pan, Sructure prediction-oriented synthesis of thiophosphates as promising infrared nonlinear optical materials, *Angew. Chem., Int. Ed.*, 2024, **63**, e202406576.

27 Y. H. Hu, X. Xu, R. X. Wang, J. Y. Han, S. S. Zhang, S. H. Zhang, J. Y. Guo, L. M. Wu and L. Chen, $[Sn_3OF]PO_4$ vs $[Sn_3F_3]PO_4$: Enhancing birefringence through breaking R3 symmetry and realigning lone pairs, *Inorg. Chem. Front.*, 2024, **11**, 5648–5656.

28 Y. Chu, P. Wang, H. Zeng, S. C. Cheng, X. Su, Z. H. Yang, J. J. Li and S. L. Pan, $Hg_3P_2S_8$: A new promising infrared nonlinear optical material with a large second-harmonic generation and a high laser-induced damage threshold, *Chem. Mater.*, 2021, **33**, 6514–6521.

29 Z. Li, S. Z. Zhang, Z. W. Huang, L. D. Zhao, E. Uykur, W. H. Xing, Z. S. Lin, J. Y. Yao and Y. C. Wu, Molecular construction from $AgGaS_2$ to $CuZnPS_4$: Defect-induced second harmonic generation enhancement and cosubstitution-driven band gap enlargement, *Chem. Mater.*, 2020, **32**, 3288–3296.

30 P. Kubelka and F. Munk, An article on optics of paint layers, *Tech. Phys.*, 1931, **12**, 593–609.

31 W. F. Zhou, J. J. Wu, W. L. Liu and S. P. Guo, Ag-based chalcogenides and derivatives as promising infrared nonlinear optical materials, *Coord. Chem. Rev.*, 2023, **477**, 214950.

32 L. H. Gao, Y. Chu, X. W. Wu, B. B. Zhang and K. Wu, From thiophosphate to chalcohalide: Mixed-anion AgS_xCl_y ligands concurrently enhancing nonlinear optical effects and laser-damage threshold, *Chem. Commun.*, 2021, **57**, 8218–8221.

33 S. Cho, X. J. Zhang, B. Lee, J. S. Kang, B. J. Jeong, D. Kim, Y. H. Kim, J. H. Park, S. H. Kim, H. K. Yu and J. Y. Choi, One-dimensional van der waals material $SbPS_4$ with large bandgap for UV sensing applications, *Sens. Actuators, A*, 2024, **376**, 115550.

34 C. Y. Zhao, B. B. Zhang, X. Y. Tian, G. Q. Zhou, J. J. Xu and K. Wu, $Na_6Sn_3P_4S_{16}$: Sn(II)-chelated PS_4 groups inspired an ultra-strong SHG response, *Inorg. Chem. Front.*, 2023, **10**, 5726–5733.

35 (*a*) Y. K. Lian, R. A. Li, X. Liu, L. M. Wu and L. Chen, $Sr_6(Li_2Cd)A_4S_{16}$ (A = Ge, Sn): How to go beyond the band gap limitation via site-specific modification, *Cryst. Growth Des.*, 2020, **20**, 8084–8089; (*b*) R. A. Li, Q. Q. Liu, X. Liu, Y. Liu, X. Jiang, Z. Lin, F. Jia, L. Xiong, L. Chen and L. M. Wu, $Na_2Ba[Na_2Sn_2S_7]$: Structural tolerance factor-guided NLO performance improvement, *Angew. Chem., Int. Ed.*, 2023, **62**, e202218048; (*c*) Q. Q. Liu, X. Liu, M. Z. Li, R. X. Wang, B. X. Li, L. M. Wu and L. Chen, $LiLnGeS_4$ (Ln = La–Nd): Designing high performance infrared nonlinear optical sulfides through "band reformation of AGS", *Angew. Chem., Int. Ed.*, 2024, e202415318.

36 V. Julien, L. Stephan, A. Mayeul, Z. Alex, Z. Andriy, F. Jason and T. Janet, Band-structure, optical properties, and defect physics of the photovoltaic semiconductor SnS, *Appl. Phys. Lett.*, 2012, **100**, 032104.

37 K. Vipin, H. J. Jeon, K. Pushpendra, G. T. Le, A. Rajeev and S. G. Jin, Anisotropic properties of two-dimensional (2D) tin dihalide (SnX_2, X = Cl, Br, I) monolayer binary materials, *J. Phys.: Condens. Matter*, 2024, **36**, 115701.

38 A. Kyono, M. Kimata, M. Matsuhisa, Y. Miyashita and K. Okamoto, Low-temperature crystal structures of stibnite implying orbital overlap of Sb $5s^2$ inert pair electrons, *Phys. Chem. Miner.*, 2002, **29**, 254–260.

39 J. P. Perdew, K. A. Jackson, M. R. Pederson, D. J. Singh and C. Fiolhais, Erratum: Atoms, molecules, solids, and surfaces: Applications of the generalized gradient approximation for exchange and correlation, *Phys. Rev. B:Condens. Matter Mater. Phys.*, 1993, **46**, 4978.

40 J. P. Perdew, K. Burke and M. Ernzerhof, Generalized gradient approximation made simple, *Phys. Rev. Lett.*, 1996, **77**, 3865–3868.

41 J. Heyd, G. E. Scuseria and M. Ernzerhof, Hybrid Functionals Based on a Screened Coulomb Potential, *J. Chem. Phys.*, 2003, **118**, 8207–8215.

42 J. Heyd, G. E. Scuseria and M. Ernzerhof, Erratum: Hybrid functionals based on a screened coulomb potential, *J. Chem. Phys.*, 2006, **124**, 219906.